The NMR Structure and Dynamics of the Two-Domain Tick Carboxypeptidase Inhibitor Reveal Flexibility in Its Free Form and Stiffness upon Binding to Human Carboxypeptidase B[†,‡]

David Pantoja-Uceda,[§,||] Joan L. Arolas,[||,⊥] Pascal García,[@,#] Eva López-Hernández,[@] Daniel Padró,[@,+] Francesc X. Aviles,*[,⊥] and Francisco J. Blanco*[,▽]

Instituto de Química-Física Rocasolano, CSIC, Serrano 119, 28006 Madrid, Spain, NMR Group, Structural Biology and Biocomputing Programme, Centro Nacional de Investigaciones Oncológicas, CNIO, Melchor Fernández Almagro 3, 28029 Madrid, Spain, Institut de Biotecnologia i Biomedicina and Departament de Bioquímica i Biologia Molecular, Universitat Autònoma de Barcelona, 08193 Bellaterra, Barcelona, Spain, and Structural Biology Unit, CIC bioGUNE, Parque Tecnológico de Bizkaia, Edificio 800, 48160 Derio, Spain

Received March 7, 2008; Revised Manuscript Received April 28, 2008

ABSTRACT: The structure of the tick carboxypeptidase inhibitor (TCI) and its backbone dynamics, free and in complex with human carboxypeptidase B, have been determined by NMR spectroscopy. Although free TCI has the same overall fold as that observed in the crystal structures of its complexes with metallocarboxypeptidase types A and B, there are structural differences at the linker between the two domains. The linker residues have greater flexibility than the globular domains, and the C-terminal residues are highly flexible in free TCI. Upon formation of a complex with carboxypeptidase B, TCI becomes more rigid, especially at the level of the linker and at the C-terminus, which is inserted into the active site groove of the carboxypeptidase. Solvent exchange rates of the backbone amide protons also show a strong reduction of the local TCI dynamics and a stabilization of its structure upon complex formation. The findings are consistent with a recognition mechanism that primarily involves the C-terminal domain, which adjusts its conformation and that of the linker, thus facilitating complex stabilization by further interactions between the N-terminal domain and an exosite of the carboxypeptidase. This adaptability enables TCI to tune its global conformation for proper interaction with distinct types of carboxypeptidases by a mechanism of induced fit. Our results provide new information about the structure−function relationship and stability of a molecule with potential biomedical applications in thrombolytic therapy. Furthermore, the plasticity of TCI makes it an ideal scaffold for developing stronger and/or more specific inhibitors directed toward modulating the activity of metallocarboxypeptidases.

Metallocarboxypeptidases (MCPs)[1] are zinc-containing exopeptidases that catalyze the hydrolysis of C-terminal amino acids from proteins and peptides. These enzymes perform many vital functions in a wide variety of organisms, ranging from food digestion or the biosynthesis of peptides that participate in intracellular signaling to the inhibition of fibrinolysis (*1*). Mammalian MCPs have been traditionally subdivided into the A/B (M14A) and N/E (M14B) subfamilies on the basis of structural and sequence similarities. The A/B subfamily includes various proteins: (1) pancreatic digestive enzymes CPA1, CPA2, and CPB; (2) mast cell CPA3, related to inflammatory processes; (3) plasma CPB (also known as TAFI, thrombin-activatable fibrinolysis inhibitor), linking blood coagulation and fibrinolytic cascades; and (4) various other genes, the precise functions of which are still unknown (*2*). In the N/E subfamily, there are enzymes that function in the biosynthesis of peptide hormones and neurotransmitters and others that do not appear to have CP activity, due to the absence of critical active site residues (*3, 4*). Although most MCPs function either within

[†] This work was supported by the Ministerio de Educación y Ciencia, Spain, Grants GEN2003-20642-C09-02 (to F.X.A. and F.J.B.) and BIO2007-68046 (to F.X.A.), by EU Grant 3D repertoire, Contract LSHG-CT-2005-512028 (to F.J.B.), and by the European Commission FPVI, Project CAMP, LSHG-2006-018830 (to F.X.A.). F.J.B. acknowledges Ikerbasque (Basque Foundation for Science) for financial support. D.P.-U. and J.L.A. were supported by Juan de la Cierva research contracts awarded by the Ministerio de Educación y Ciencia, Spain.

[‡] The coordinates and NMR restraint file have been deposited in the Protein Data Bank as entry 2JTO, and the NMR chemical shifts have been deposited in the BioMagResBank as entry 15372.

* To whom correspondence should be addressed. F.X.A.: telephone, 34-935811315; fax, 34-935812011; e-mail, francescxavier.aviles@uab.es. F.J.B.: telephone, 34-946572521; fax, 34-946572502; e-mail, fblanco@cicbiogune.es.

[§] CSIC.

[||] These authors contributed equally to this work.

[⊥] Universitat Autònoma de Barcelona.

[@] CNIO.

[#] Present address: Oncura, Orense 85, 28020 Madrid, Spain.

[+] Present address: CICbiomaGUNE, Paseo Miramón 182, 20009 San Sebastián, Spain.

[▽] CIC bioGUNE.

[1] Abbreviations: bCPA, bovine carboxypeptidase A; CSP, chemical shift perturbation; DSS, 2,2-dimethyl-2-silapentane-5-sulfonate sodium salt; ΔG_{ex}, free energy of exchange; hCPB, human carboxypeptidase B; HSQC, heteronuclear single-quantum coherence; LCI, leech carboxypeptidase inhibitor; MCP, metallocarboxypeptidase; PCI, potato carboxypeptidase inhibitor; rmsd, root-mean-square deviation; TAFI, thrombin-activatable fibrinolysis inhibitor; TCI, tick carboxypeptidase inhibitor.

10.1021/bi800403m CCC: $40.75
Published on Web 06/18/2008

the secretory pathway or after secretion outside the cell, a new subfamily of cytosolic MCPs that are thought to process tubulin has recently been discovered (*5, 6*). This broadens the physiological role of these enzymes toward novel functions (i.e., in the cytoskeleton) and stresses their importance as potential pharmaceutical targets (*7*).

Compared with other peptidase families, only a few proteinaceous inhibitors have been reported for MCPs (*8*). Among them, the potato and leech carboxypeptidase inhibitors (PCI and LCI, respectively) have been extensively characterized in terms of folding and inhibitory activity (*9, 10*). The unbound PCI and LCI inhibitor structures have been determined by NMR, and the structures of PCI in complex with bovine CPA and LCI in complex with human CPA2 have been determined by X-ray crystallography (*11–13*). The structures of these complexes show that both molecules inhibit the MCPs through their C-terminal tails in a substratelike manner. The carboxypeptidase inhibitor from ticks (TCI) has recently been identified and characterized (*14*). TCI is 75 residues long, larger than LCI and PCI, and displays lower inhibition constants against MCPs of the A/B subfamily. Interestingly, its strong inhibition of human TAFI ($K_i = 1.2$ nM) serves to stimulate the fibrinolysis of clots; this in turn helps maintain the liquid state of blood (*1*), a natural function inside the hematophagous parasite. This characteristic makes it a promising coadjuvant for thrombolytic therapies based on the tissue-type plasminogen activator. TCI is a disulfide-rich protein with six disulfide bridges that strongly constrain its structure and contribute to its extremely high stability against temperature and denaturing agents (*14, 15*). Although the structure of free TCI is not known, the crystal structures of its complexes with two MCPs, bovine CPA (the archetype CP) and human CPB (a TAFI homologue), have shown the presence of two globular domains in TCI that are structurally similar, despite their low level of sequence homology (*16*). These structures have also revealed a novel double-headed binding mode not previously observed for the other known MCP inhibitors. The C-terminal tail of TCI inserts into the active site groove of the enzyme, and the N-terminal domain anchors to an exosite located on the CP surface.

We report the high-resolution structure of TCI free in solution. We also report on its backbone dynamics, both free and in complex with human CPB, using NMR spectroscopy. The differences in the structure, dynamics, and stability of TCI arising from binding the carboxypeptidase were analyzed in detail. The TCI protein structure in its free state has a two-domain fold similar to that in the complex. However, differences were observed between both forms, mostly caused by the different dynamics of TCI upon binding of the target carboxypeptidase. These results provide further insight into the structure−function relationship of a molecule that could be used as a scaffold for engineering inhibitors with novel specificities and as a profibrinolytic drug.

MATERIALS AND METHODS

Protein Expression and Purification. The recombinant expression of TCI was carried out as previously reported (*14*). Uniformly labeled [^{15}N]TCI was expressed by growing cells in M9 medium containing $^{15}NH_4Cl$ as the only nitrogen source. For the production of the uniformly ^{13}C- and ^{15}N-labeled sample, a defined minimal medium was used (*17*) with [$^{13}C_6$]glucose and $^{15}NH_4Cl$ as the only carbon and nitrogen sources, respectively. Purification of the expressed proteins was conducted as described previously (*14, 15*). Maximal purity (>98%) was achieved by loading the protein on a gel-filtration column (Superdex Peptide, GE Healthcare) using 30% acetonitrile as the solvent. The protein identity and purity were confirmed by mass spectrometry and automated Edman degradation, respectively. Final protein samples were kept lyophilized. Recombinant human pro-CPB was produced as previously described in detail (*18*). Active hCPB (309 residues) was obtained by a controlled activation process with bovine trypsin (Sigma), using a 1:100 (w/w) enzyme:substrate ratio at 4 °C for 24 h. Purification was monitored by SDS−PAGE, and the prosegment was separated from the active enzyme by ultrafiltration using a 30 kDa Amicon apparatus (Millipore). Complex formation resulted in the His residue at the C-terminus of TCI being processed.

NMR Samples and Spectroscopy. TCI NMR samples were prepared by dissolving the lyophilized protein powder in 300 or 600 μL of a H_2O/D_2O mixture (19:1, ratio by volume), containing 50 μM 2,2-dimethyl-2-silapentane-5-sulfonate sodium salt (DSS) as the internal reference for ^{1}H chemical shifts. The pH was adjusted to 5.5 with concentrated NaOH or HCl. The TCI−hCPB crystal structure had been previously determined at this pH (*16*). We used three protein samples for spectral assignment and structure determination: (1) 0.76 mM unlabeled protein, (2) 1.05 mM protein uniformly labeled with ^{15}N, or (3) 0.1 mM protein uniformly labeled with ^{13}C and ^{15}N. The TCI−hCPB complex sample was prepared by incubating equimolar quantities of [^{15}N]TCI and activated hCPB (2 and 8 mg, respectively) in 2 mM Tris-HCl buffer (pH 7.0) at 25 °C for 2 h. The almost complete inhibition of the enzyme was confirmed by a continuous spectrophotometric assay at 350 nm with the chromogenic substrate *N*-(4-methoxyphenylazoformyl)-Arg-OH (Bachem). The sample was concentrated to 300 μL by ultrafiltration (Amicon), readjusted to pH 5.5, and mixed with D_2O (19:1, final ratio by volume) to a final protein concentration of 0.8 mM. For the amide proton exchange experiments, the samples were lyophilized and resuspended in D_2O.

NMR experiments were performed at 298 K on a Bruker AV 700 spectrometer or on a Bruker AV 600 spectrometer equipped with a cryoprobe. Sequence-specific polypeptide backbone and side chain chemical shift assignments were made using the following experiments: TOCSY, NOESY, COSY, ^{1}H−^{15}N HSQC, ^{13}C−^{1}H HSQC, HNCO, HNCACB, CBCA(CO)NH, HNHA, HNHB, (H)CC(CO)NH, ^{1}H−^{15}N TOCSY-HSQC, and ^{15}N-edited NOESY-HSQC (*19*). Distance restraints were collected from the homonuclear and ^{15}N-edited NOESY spectra recorded with a mixing time of 150 ms. Backbone ^{1}H and ^{15}N chemical shift assignments of the TCI−hCPB complex were made using ^{1}H−^{15}N HSQC and^{15}N-edited NOESY-HSQC (80 ms mixing time) spectra recorded on uniformly ^{15}N-labeled TCI at 298 and 308 K. NMRPipe (*20*) and NMRView (*21*) were used to process raw NMR data and for interactive spectrum analysis, respectively. Chemical shifts were referenced to DSS used as an internal reference for ^{1}H and were calculated for ^{15}N and ^{13}C (*22*). Chemical shift perturbations resulting from complex formation were calculated using the equation CSP

$= [(\Delta\delta_H)^2 + (\Delta\delta_N/5)^2 \times 0.5]^{1/2}$ (*23*), in which $\Delta\delta_H$ and $\Delta\delta_N$ are the chemical shift changes in the ^1H and ^{15}N resonances, respectively. The threshold for significant changes (0.03 ppm) was calculated using the spectral resolutions in the ^1H and ^{15}N acquisition dimensions of the HSQC spectra as the values for $\Delta\delta_H$ and $\Delta\delta_N$, respectively.

Structure Calculation. Peak lists for the NOESY spectra were generated by interactive peak picking, and peak volumes were determined with the automatic integration function of NMRView (*21*). The three-dimensional structure was determined by combined automated NOESY cross-peak assignment (*24*) and structure calculation with torsion angle dynamics (*25*) implemented in CYANA (*26*). The standard CYANA protocol of seven iterative cycles of NOE assignment and structure calculation, followed by a final structure calculation, was applied. Stereospecific assignments for 29 isopropyl methyls and methylene groups were determined using the GLOMSA method (*27*) before the final structure calculation by analyzing the structures obtained in the preceding calculation cycles. Additionally, as TCI contains 12 cysteine residues involved in disulfide bridges, six sets of standard upper and lower limits for each identified bond, 2.1/2.0 Å for $S_\gamma(i)-S_\gamma(j)$ and 3.1/3.0 Å for $C_\beta(i)-S_\gamma(j)$ and $S_\gamma(i)-C_\beta(j)$, were introduced during the structure calculation cycles. Weak constraints on φ and ψ torsion angle pairs and on side chain torsion angles between tetrahedral carbon atoms were used temporarily during the NOE assignment−structure calculation cycles to favor allowed regions of the Ramachandran plot and staggered rotamer positions, respectively (*28*). The 15 backbone hydrogen bonds that were consistently present in the preliminary ensemble of structures, and whose amide protons were found to be protected from solvent exchange in D_2O, were included as constraints in the final round of structure calculations. The 20 conformers with the lowest final CYANA target function values were subjected to restrained energy minimization in vacuo with AMBER7 (*29*). The structural quality of the final structures was evaluated with PROCHECK-NMR, which also provided an average structure of the NMR ensemble (*30*). MOLMOL (*31*) was used to visualize the structures and prepare the figures.

^{15}N Relaxation Measurements and Analysis. ^{15}N T_1 and T_2 values and $\{^1H\}-^{15}N$ NOE spectra (*32*) for free TCI were acquired at 600 MHz, pH 5.5, and 298 K on a 0.7 mM uniformly ^{15}N-labeled sample. Eight delays (20, 60, 240, 360, 460, 660, 860, and 1100 ms) were used for T_1 measurements, and a different set of seven delays (16, 31, 63, 110, 221, 270, and 396 ms) was used to measure the T_2 values. $\{^1H\}-^{15}N$ NOE experiments were carried out with an overall recycling delay of 10 s to ensure the maximal development of NOEs before acquisition and to allow solvent relaxation, thus avoiding transfer of saturation to the most exposed amide protons of the protein between scans (*33*). $\{^1H\}-^{15}N$ NOE, T_1, and T_2 experiments for TCI bound to hCPB were carried out under conditions similar to those of free TCI, but with twice the number of scans and with different sampling times. Six delays (20, 460, 860, 1260, 1600, and 2200 ms) were used for T_1 measurements and five delays (0, 16, 31, 47, 63, and 79 ms) for T_2. Relaxation times were calculated via least-squares fitting of peak intensities to a two-parameter exponential function, using the rate analysis routine of the java version of NMRView (*34*). Heteronuclear NOEs were calculated from the ratio of cross-peak intensities in spectra collected with and without amide proton saturation during the recycle delay. Uncertainties in peak heights were determined from the standard deviation of the distribution of intensities in the region of the HSQC spectra where no signal and only noise was observed.

The principal components of the TCI inertia tensor were calculated with Pdbinertia (A. G. Palmer, III, Columbia University, New York, NY) using the average NMR structure for free TCI, and the X-ray structure (*16*) for the TCI−hCPB complex. We estimated the overall correlation time from the ratio of the mean values of T_1 and T_2. The values for T_1 and T_2 were calculated from a subset of residues with little internal motion and no significant exchange broadening. This subset excluded residues with NOEs of <0.65 and also residues with T_2 values lower than the average minus one standard deviation, unless their corresponding T_1 values were larger than the average plus one standard deviation (*35*). The diffusion tensor, which describes rotational diffusion anisotropy, was determined by two approaches (*36, 37*): the r2r1_diffusion program and the quadric_diffusion program (A. G. Palmer, III, Columbia University). The calculations were unsuccessful after using the errors in T_1 and T_2 estimated by Monte Carlo simulations; these were unrealistically low. Therefore, the errors were scaled up by the minimum factor allowing an interpretation of the data in terms of a rotational diffusion tensor. This procedure resulted in average errors of 5% (free TCI) and 15% (bound TCI). The ^{15}N relaxation was analyzed assuming dipolar coupling with the directly attached proton (with a bond length of 1.02 Å), and a contribution from the ^{15}N chemical shift anisotropy evaluated as −160 ppm. Relaxation data were fitted to the Lipari and Szabo model (*38*) using FAST-Modelfree (*39*), which interfaces with MODELFREE version 4.2 (*40*). Five models of internal motion were evaluated for each amide $^1H-^{15}N$ pair: (i) S^2, (ii) S^2 and τ_e, (iii) S^2 and R_{ex}, (iv) S^2, τ_e, and R_{ex}, and (v) S_f^2, S^2, and τ_e, where S^2 is the generalized order parameter, τ_e is the effective internal correlation time, R_{ex} is the exchange contribution to transverse relaxation, and S_f^2 is related to the amplitude of the fast internal motions.

Amide Proton Exchange Measurements and Analysis. The exchange of the TCI amide protons for solvent deuterons was measured at pH 5.5 and 298 K. The exchange reaction was initiated by dissolving a lyophilized sample of ^{15}N-labeled TCI in 300 μL of 99.98% D_2O to a final protein concentration of ~0.7 mM. The first $^1H-^{15}N$ HSQC spectrum was acquired within 25 min of the initiation of exchange. Successive $^1H-^{15}N$ HSQC spectra with a duration of 19.5 min were collected using a fast version of the HSQC experiment (*41*) over the course of 4 days. Amide exchange experiments for TCI bound to hCPB were conducted for 76 min each to increase the signal-to-noise ratio in the spectra of this sample, which exhibited signals broader than those of free TCI. The first spectrum was acquired 39 min after the initiation of exchange, and successive spectra were acquired over a time period of 14 days. The same processing scheme was applied to all spectra. Hydrogen exchange rates were determined by fitting the decay in cross-peak intensities versus time to the single-exponential equation $I = A \exp(-k_{ex}t) + C$ using the rate analysis module of NMRView (*34*), where I represents the intensity of the cross-peak, A is the amplitude of the exchange curve, k_{ex} is the observed exchange rate, t is the time after adding D_2O, and C is a

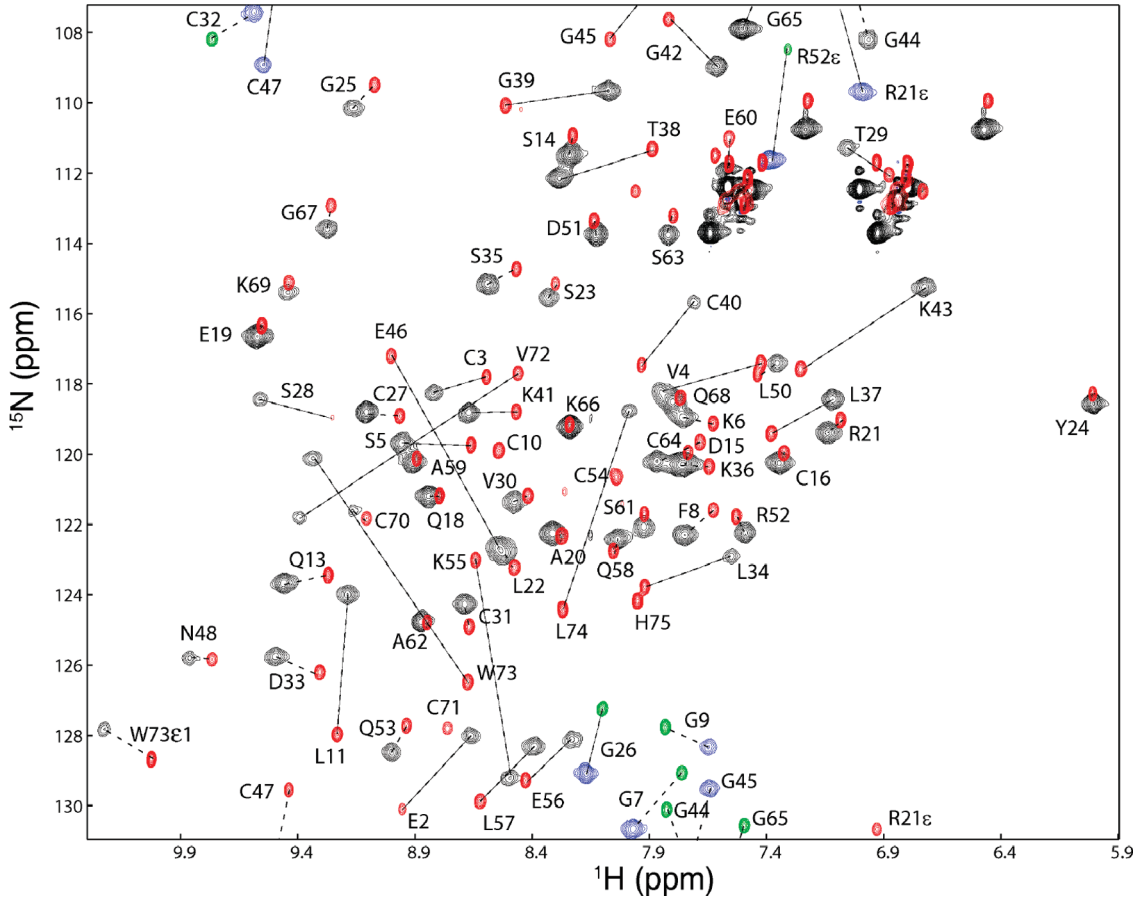

FIGURE 1: Overlay of the NMR ^{1}H−^{15}N HSQC spectra of uniformly ^{15}N-labeled TCI, free (red and green) and bound to hCPB (black and blue) at pH 5.5 and 298 K. Cross-peaks are labeled with their corresponding residue number and single-letter code. Peaks that are folded in the ^{15}N dimension are colored green and blue for TCI and the TCI−hCPB complex, respectively. For residues Cys10, Cys54, and Cys71, no assignment could be made in the complex form. Signals without labels correspond to amides from the side chains of Asn and Gln residues.

constant which takes into account the residual nondeuterated water. The k_{ex} upper or lower limit values for amide protons that were absent or very weak in the first experiment or that apparently had an unchanged intensity in the last recorded HSQC spectrum were estimated taking into account the duration of the first experiment, the accumulated time until the last one displaying observable cross-peak intensities, and a conservative assumption regarding the sensitivity of our measurements. Assuming that remaining intensities or signal decays of <10% could not be reliably measured, the fastest exchanging amide protons in free TCI had a k_{ex} of $\geq 9 \times 10^{-2}$ min^{-1}. For TCI bound to hCPB, in which some signals remained apparently unchanged after 14 days, the interval of measurable exchange rates was from 5×10^{-6} to 3×10^{-2} min^{-1}. Under an EX2 exchange mechanism (see the Supporting Information), the apparent free energies of exchange can be calculated from the equation $\Delta G_{ex} = -RT \ln(k_{ex}/k_{int})$, where R is the gas constant and T the absolute temperature. The intrinsic exchange constant, k_{int}, was calculated for every amino acid of the TCI sequence using the web tool available at www.fccc.edu/research/labs/roder/sphere (*42*).

RESULTS

NMR Assignments and Secondary Structure of TCI. The backbone ^{1}H, ^{15}N, and ^{13}C resonances of TCI were assigned by the conventional sequential assignment strategy using triple-resonance experiments (*19*). The ^{1}H−^{15}N HSQC spectrum of TCI displayed a very well dispersed set of narrow signals (Figure 1), as expected for a small folded polypeptide chain. The major set of 72 backbone ^{1}H and ^{15}N cross-peaks was unambiguously assigned to one of the 75 residues of TCI, with the exception of Asn1, Pro12, Pro17, and Pro49, for which no correlation was expected. Three automated assignment programs based on various approaches (*43–45*) yielded results similar to those of the manual assignment. Further analysis of the TOCSY and NOE data permitted a nearly complete ^{1}H side chain assignment, with the only exceptions being some distal side chain resonances of Arg and Lys residues. Overall, 95.7% of the chemical shifts of the nonlabile protons and backbone amide protons were assigned, including 87.0% of the ^{15}N and ^{13}C nuclei resonances.

The ^{1}H−^{15}N HSQC spectrum of TCI bound to hCPB was overlaid with that of free TCI (Figure 1). The cross-peaks in the spectrum of bound TCI were much broader than those in its free state, because of the increased molecular mass (from 8 to 42 kDa in the complex) and concomitant shorter transverse relaxation times (see below). Backbone ^{1}H and ^{15}N resonance assignments for TCI bound to hCPB were based on the comparison of the ^{1}H−^{15}N HSQC spectra for free and complex forms of TCI, and ^{15}N-edited NOESY-HSQC spectra of the complex recorded at 298 and 308 K. All cross-peaks were assigned to a TCI residue, but three

residues (Cys10, Cys54, and Cys71, which are located at the TCI−hCPB interface) were not observed in the spectrum. The C-terminal His75 residue was also absent in the NMR spectrum of bound TCI, because it is processed upon binding of the carboxypeptidase (*16*).

For all Xxx−Pro peptide bonds, the trans conformation was confirmed independently by intense Xxx (H_α)−Pro (H_δ) sequential NOEs (*46*) and by the $^{13}C_\beta$ and $^{13}C_\gamma$ chemical shift differences (*47*). The individual covalent links between the cysteine residues that form the six disulfide bridges in TCI were identified by careful analysis of the NOESY spectra. Several inter-cysteine NOE connectivities allowed us to clearly identify two disulfide bonds in each domain: Cys10−Cys27 (H_α, $H_{\beta2}$−$H_{\beta2}$; $H_{\beta3}$−H_α), Cys16−Cys32 ($H_{\beta3}$−$H_{\beta3}$), Cys47−Cys64 (H_α−$H_{\beta3}$), and Cys54−Cys71 ($H_{\beta2}$, $H_{\beta3}$−$H_{\beta3}$). These and the two other disulfide bonds (Cys3−Cys31 and Cys40−Cys70) were confirmed by long-range NOEs observed between residues in the vicinity of the cysteines (see Figure S1 of the Supporting Information). This pairing is consistent with the set of disulfide bonds identified from the crystal structure of TCI in complex with two different carboxypeptidases (bCPA and hCPB) (*16*).

Structure of TCI in Solution. Of the 3177 cross-peaks that were identified in the two-dimensional (2D) NOESY and three-dimensional (3D) $^1H-^{15}N$ NOESY-HSQC spectra, 93% could be assigned with CYANA (*24, 26*). Sixty-seven dihedral angle constraints derived from quantitative analysis of the HNHA spectrum (*48*) and the backbone chemical shifts using TALOS (*49*) were also added to the calculations. An average of 17 constraints per residue was used in the final structure calculation. The 20 energy-minimized conformers represent the structure of TCI in solution. Statistics for the quality and precision of this ensemble are summarized in Table 1. The ensemble of NMR structures is highly consistent with the experimental data, with no distance constraint violations larger than 0.25 Å. The high quality of the structures is indicated by the distribution of the φ and ψ backbone torsion angles, which are all in the most favored regions or in the additionally allowed regions of the Ramachandran map (see Table 1). The secondary structure of TCI consists of short helices and β-strands, which are indicated in Figure 2A. This figure also summarizes the observed sequential and short-range NOEs, and the protection against exchange of the amide protons.

The global fold of TCI in solution consists of two globular domains (Figure 2B,C). The N-terminal domain spans residues 1−36; the C-terminal domain includes residues 39−75, and the interdomain linker consists of residues 37 and 38. The TCI N-terminal domain has a one-turn α-helix ($\alpha1_N$, Cys3−Lys6) and a central antiparallel β-sheet as secondary structure elements. The β-sheet constitutes the core of this domain and is formed by three β-strands, $\beta1_N$ (Gly9−Leu11), $\beta2_N$ (Arg21 and Leu22), and $\beta3_N$ (Val30−Cys32). The TCI C-terminal domain also contains a one-turn α-helix, $\alpha1_C$ (Cys40−Lys43), and a central three-stranded antiparallel β-sheet, $\beta1_C$ (Gly45−Pro49), $\beta2_C$ (Lys55 and Glu56), and $\beta3_C$ (Gln68−Val72), in which $\beta2_C$ is connected to $\beta3_C$ by a two-turn α-helix, $\alpha2_C$ (Gln58−Cys64). Other parts of the polypeptide chain consist of coil and turn structures, with a well-defined type II β-turn at residues Asp33−Lys36. The structure of the domains is compact and stable, as illustrated by the protection of the amide backbone protons (Figure 2A); many of these protons are detected and persist in the presence of deuterated water due to their participation in hydrogen bonds and/or their burial and reduced solvent accessibility. As shown in the space-filling model of TCI (Figure 2C), a crown of charged residues (Lys41, Glu46, Arg52, and Lys55) surrounds the C-terminal tail. In the complexes with bCPA and hCPB, this region covers the carboxypeptidase active site, in which the C-terminal tail of TCI interacts with the active site of the enzyme in a way that mimics substrate binding, while the N-terminal domain binds to an exosite separated from the active site groove (*16*).

Table 1: Structural Statistics of the 20 Best NMR Structures of TCI

NOE Distance Constraints	
no. of intraresidual distances	281
no. of sequential distances	376
no. of medium-range distances ($i - j < 5$)	237
no. of long-range distances ($i - j \geq 5$)	325
no. of angular restraints	67
total	1286
final CYANA target function value[a] (Å^2)	0.10
maximum distance restraint violation (Å)	0.25
AMBER energy[b] (kcal/mol)	−1244

Root-Mean-Square Deviations from Ideal Geometry	
bond lengths (Å)	0.01
bond angles (deg)	2.01

Root-Mean-Square Deviations from Mean Coordinates (Å)			
	residues 2−74	residues 2−36	residues 39−74
backbone N, C^α, C′	1.69	0.24	0.56
all heavy atoms	2.25	0.93	1.55

Ramachandran Plot Statistics (%)[c]	
most favorable regions	88.9
additional allowed regions	11.1
generously allowed regions	0.0
disallowed regions	0.0

[a] The final CYANA target function value was computed for the structure before energy minimization with AMBER. [b] Average values over the 20 final energy-minimized CYANA conformers. [c] Calculated with PROCHECK-NMR (*30*).

The convergence among the 20 NMR structures, as measured by the root-mean-square deviation (rmsd) values from the mean coordinates (Table 1), was very high for each individual domain, but it was smaller for the C-terminal one, caused partly by the increased flexibility of the C-terminal residues (see below). However, the convergence for the structure as a whole was much lower, even though the turn structure at the linker itself was well-defined by experimental restraints; these are illustrated by the various superimpositions of NMR structures (Figure 3). The two domains were well separated from each other in solution, as no NOEs were detected between them. Also, no NOEs were observed between the linker residues and the rest of the protein, as one can see in the NOE contact map (see Figure S1 of the Supporting Information). This suggests that the linker has partial flexibility and may explain the structural divergence in the NMR ensemble. The structural alignment statistics comparing the average NMR structure of free TCI with the X-ray structures of TCI in complex with bCPA and hCPB are presented in Table 2, and the structure superimpositions with hCPB are shown in Figure 3. The small rmsd values

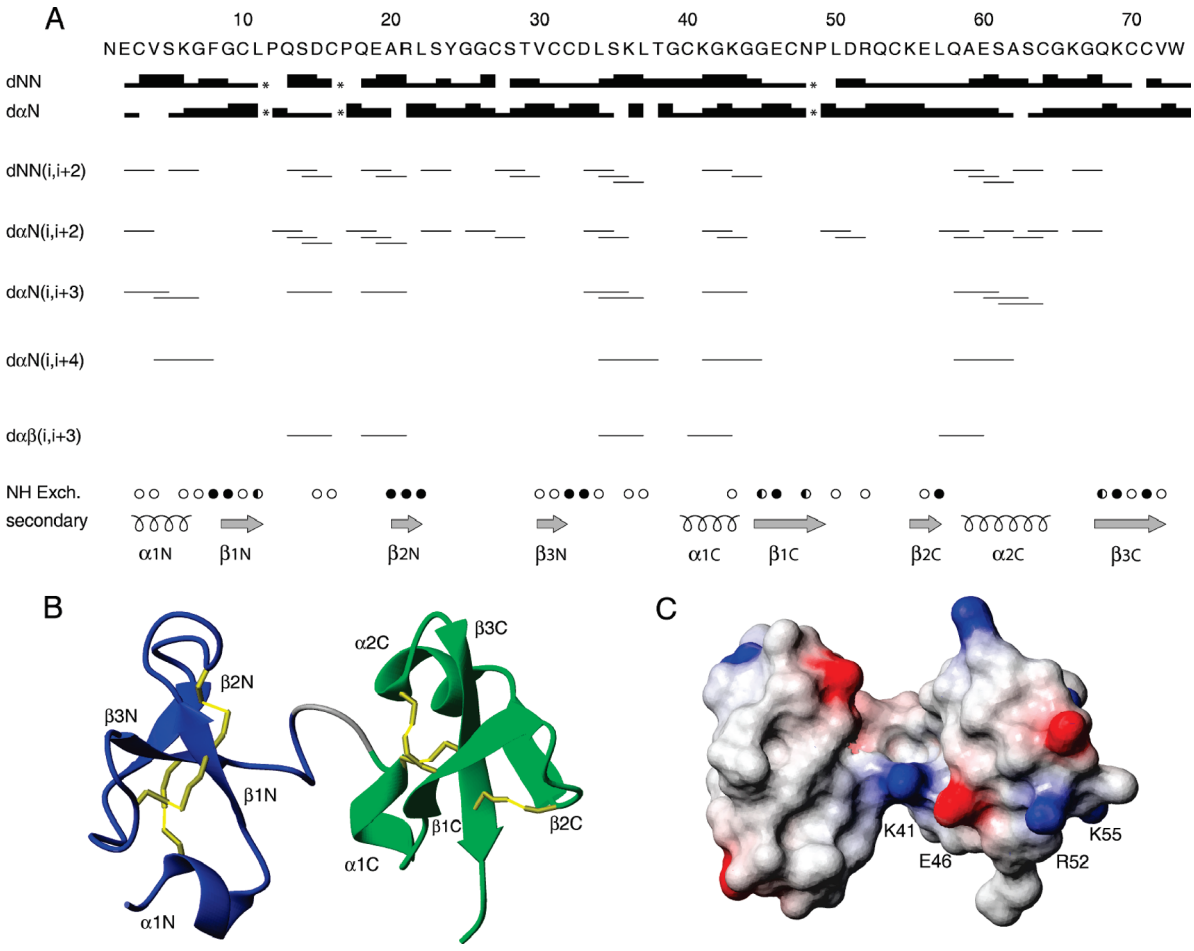

FIGURE 2: Solution structure of free TCI. (A) Short-range NOEs, secondary structure, and amide proton exchange data for free TCI. The thickness of the sequential NOEs indicates their relative intensity according to three categories (strong, medium, and weak). Empty circles denote residues of which amide protons were observed in the first HSQC spectrum recorded after dissolution of the protein in D_2O; half-filled circles indicate that the corresponding NH exchanges were complete after 15 h, and filled circles denote residues for which NH was still observed after exchange for 15 h. (B) Ribbon diagram of the average structure of TCI with the N-terminal domain colored blue (residues 1−36), the C-terminal domain green (residues 39−75), and the linker gray (residues 37 and 38). The disulfide bonds are colored yellow. (C) Space-filling representation of TCI with the surface electric potential colored blue (positive) or red (negative).

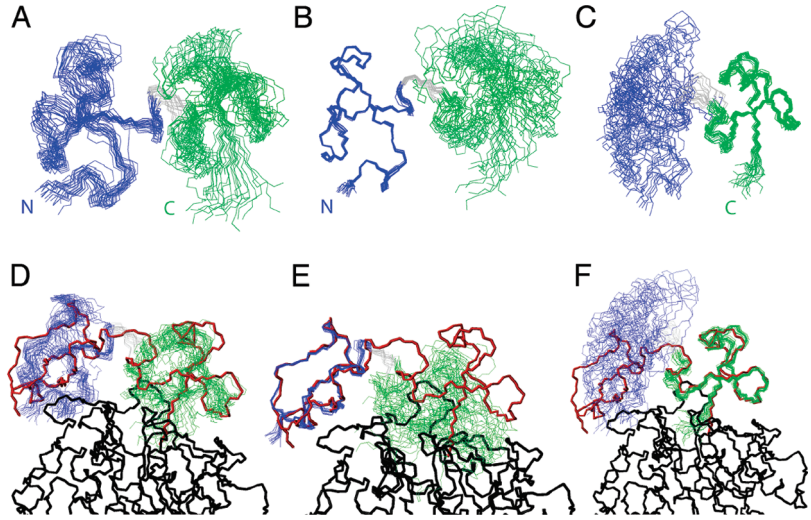

FIGURE 3: Comparison of the TCI structure in its free state and in complex with hCPB. Superposition of (A) the backbone atoms of the best 20 calculated structures for residues 2−74 of TCI, (B) the N-terminal domain of residues 2−36, or (C) the C-terminal domain of residues 39−74. In panels D−F, superpositions similar to those in panels A−C, respectively, were performed, including the X-ray structure of TCI (red line) in complex with hCPB (black line). The N-terminal domain, linker, and C-terminal residues in the NMR structures are colored blue, gray, and green, respectively.

for the C_α atoms highlight the significant similarity between the solution and crystal structures of TCI at the level of the individual domains. However, the alignment was worse if the whole TCI chain was used, suggesting that a conforma-

Table 2: Summary of the rmsds for the C_α Atoms of TCI in the NMR and Crystal Structures[a]

	NMR		
crystal	TCI (1−75)	TCI N-terminus (1−36)	TCI C-terminus (39−75)
TCI−bCPA[b]	3.6 Å	−	−
TCI−bCPA N-terminus	−	1.0 Å	−
TCI−bCPA C-terminus	−	−	1.3 Å
TCI−hCPB[c]	3.1 Å	−	−
TCI−hCPB N-terminus	−	0.9 Å	−
TCI−hCPB C-terminus	−	−	1.5 Å

[a] The structural alignment and superposition were carried out with DaliLIte (*57*). [b] Bovine carboxypeptidase A complex (PDB entry 1ZLH). [c] Human carboxypeptidase B complex (PDB entry 1ZLI).

tional change at the linker occurs upon complex formation or that one of the possible conformational states of TCI in solution is stabilized in the complex.

Backbone Dynamics from ^{15}N Relaxation of Free and Bound TCI. We measured the^{15}N relaxation parameters for the free and complex forms of TCI (Figure 4). The heteronuclear $\{^1H\}-^{15}N$ NOE and the longitudinal (T_1) and transverse (T_2) relaxation times were measured for 69 of the 75 residues of free TCI (all except the N-terminal residue, the three prolines, and Val4 and Leu50, for which signals overlap). For the TCI bound to hCPB, the relaxation data were measured for only 59 residues, because of missing signals and an increased level of overlap with respect to the spectrum for free TCI.

The average values of the ^{15}N relaxation parameters for the two forms of TCI are summarized in Table 3. There were several residues that deviated from the average, mostly at the C-terminus of free TCI, for which small NOEs (Figure 4) indicated flexibility on fast time scales (picoseconds to nanoseconds). Global rotational diffusion correlation times of 4.2 and 22.1 ns were obtained for free TCI and TCI bound to hCPB, respectively. The principal components of the TCI inertia tensor, calculated for the average NMR structure, have relative values of 1.00, 0.90, and 0.36. The corresponding values for the TCI bound to hCPB, determined from the crystal structure, are 1.00, 0.87, and 0.66, respectively; these values indicate that the shape of both species deviates from that of a sphere and approaches a prolate ellipsoid, especially so in the case of the free protein. In agreement with this finding, the diffusion tensor that better explained the relaxation data was also anisotropic, with different values for the diffusion constants parallel and orthogonal to the long axis of the molecule ($D_\parallel/D_\perp = 1.3$ for TCI and 0.7 for the TCI−hCPB complex).

The relaxation data were analyzed using the model-free formalism to calculate the corresponding dynamics parameters for the amide $^1H-^{15}N$ pair of each residue. Most ^{15}N relaxation parameters could be satisfactorily fitted to one of the two simpler models (see Materials and Methods), which describe the internal dynamics of the molecule in terms of a generalized order parameter S^2 and an effective correlation time τ_e for fast motions. In a few cases (nine residues in TCI and one in the hCPB−TCI complex), it was necessary to include a contribution of slow motions to the transverse relaxation time, on the microsecond to millisecond time scale, which are characterized in terms of conformational exchange rate R_{ex}. In other cases (seven residues in TCI and one in the hCPB−TCI complex), the inclusion of the amplitude of internal motions (S_f^2) was also necessary to obtain a good fitting. Figure 5 shows the values of S^2 and R_{ex} for each residue of free and bound TCI.

Amide Proton Exchange of Free and Bound TCI. We measured the exchange rates of backbone amide protons in 30 of the 72 TCI residues with observable amide protons (Figure 6 and Tables S1 and S2 of the Supporting Information). These values could not be determined for the other 42 residues, for various reasons. Some exchanged so fast that they could not be observed in the first HSQC; for others, the decay in the signals was too rapid and the curve could not be fitted to yield a reliable estimate of the exchange rate, and for a few, signal overlap prevented a reliable measurement. The number of measured rates for TCI bound to hCPB was even smaller, because the signals for the complex were much broader than those for the free form (Figure 1). This decreases the sensitivity of the HSQC experiments and increases the signal overlap. Only 15 NH exchange rates could be reliably measured. For another 11 residues, hardly any signal decay could be detected after exchange for 14 days. Therefore, a lower limit for the exchange rate of 3×10^{-2} min^{-1} was estimated for these residues (see Materials and Methods). For the rest of the residues, either the cross-peaks were not observed in the first HSQC after dissolution of the sample in deuterated water or an estimate of the exchange rate could not be reliably obtained because of significantly fast signal decay.

To distinguish between EX1 and EX2 exchange mechanism limits (*50, 51*), the values of k_{ex} were measured at pH 5.5 and 6.4. The plot of log k_{ex} at the two pH values showed a straight line with a slope close to 1, within experimental uncertainty (see Figure S2 of the Supporting Information), indicating an EX2 mechanism for the 12 residues for which the exchange rates could be measured at the two pH values. Furthermore, the wide range of measured k_{ex} values is consistent with an EX2 mechanism for most, if not all, residues in TCI. The pH dependence test was not performed for TCI bound to hCPB. However, an EX2 exchange regime may be assumed on the basis of the results obtained for free TCI and the spread in k_{ex} values.

DISCUSSION

TCI Structure. The structure of free TCI in solution is represented well by the ensemble of the 20 NMR-derived models. It consists of two separated globular domains, as previously observed in the X-ray structures of TCI in complex with different carboxypeptidases (*16*); the domains share no contact other than the two-residue segment linking them, the structure of which is defined only by local restraints. Even though the degree of sequence similarity is low, the two domains are structurally similar (rmsd of 1.8 Å for backbone atoms). The major differences are the lengths of the β-strands in the central β-sheets, which constitute the core of the two domains (strands $\beta1$ and $\beta3$ are two residues longer in the C-terminal domain than in the N-terminal one) and the presence of a second helix in the C-terminal domain. The overall fold shared by the two domains and their disulfide pattern are similar to those of the β-defensin fold family, as previously noted (*16*). The NMR ensemble shows a high degree of similarity for each of the two domains independently, less so for the C-terminal domain, but the

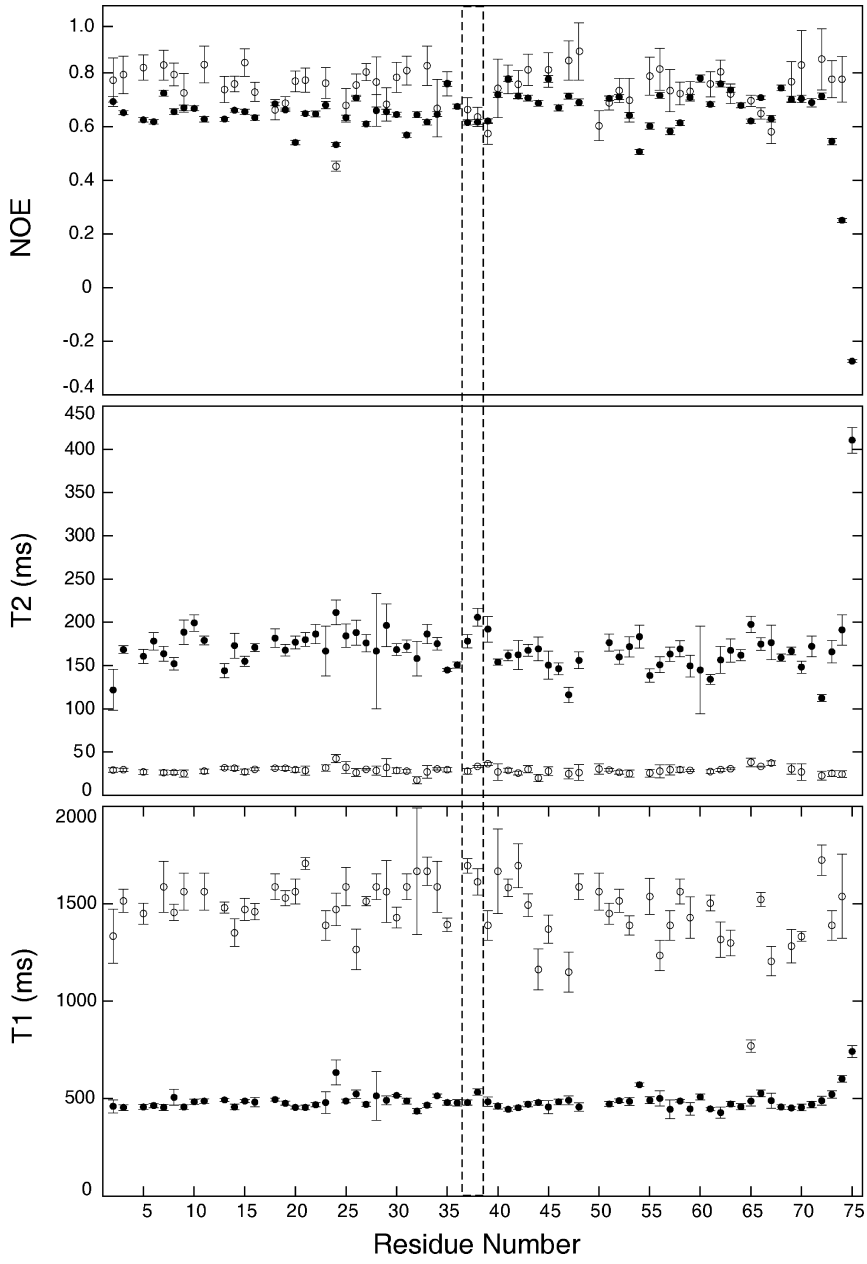

FIGURE 4: Backbone NMR relaxation data for TCI. Heteronuclear $\{^1H\}-^{15}N$ NOEs and ^{15}N transverse (T_2) and longitudinal (T_1) relaxation times are represented for each residue of TCI in its free form (●) and in complex with hCPB (○). The vertical dotted lines indicate the limits between the two domains and the linker.

Table 3: Average Values and Standard Deviations of the Measured ^{15}N Relaxation Parameters and Overall Fitted Isotropic Correlation Times for Free and Bound TCI at 298 K and 14.09 T

parameter	TCI	TCI−hCPB
$\{^1H\}-^{15}N$ NOE	0.64 ± 0.13	0.74 ± 0.08
T_1 (ms)	480 ± 5	1470 ± 160
T_2 (ms)	170 ± 3	29 ± 4

conformational heterogeneity increases when the full chain is aligned. A partially flexible linker will explain this structural divergence, which is consistent with the individual folding of the two domains determined previously (*15*).

In the crystal structures of the complexes with bCPA and hCPB (*16*), TCI has the same two-domain fold as it does free in solution. However, local differences exist between the bound and free states, particularly at the hinge between the two domains; large differences were observed in the ψ angle of residue Leu37 (see Figure S3 of the Supporting Information), which was not restrained during the structure calculations. The degree of similarity between the NMR ensemble of free TCI structures and the bound structures is very high for the individual domains but is much lower for the whole TCI molecule (Figure 3 and Table 1). This result suggests that either the linker is partly flexible in free TCI and becomes fixed in a conformation that is different from the average upon complex formation or the binding induces a conformational change in the linker. On the other hand, the degree of similarity between the structures of the free and bound forms of TCI is higher for the N-terminal domain than for the C-terminal one (see Table 2), indicating that the conformation of the C-terminal domain is more affected by complex formation than that of the N-terminal domain. This is consistent with the pattern of chemical shift perturbation (CSP) values arising from the binding of TCI to hCPB (Figure S4 of the Supporting Information).

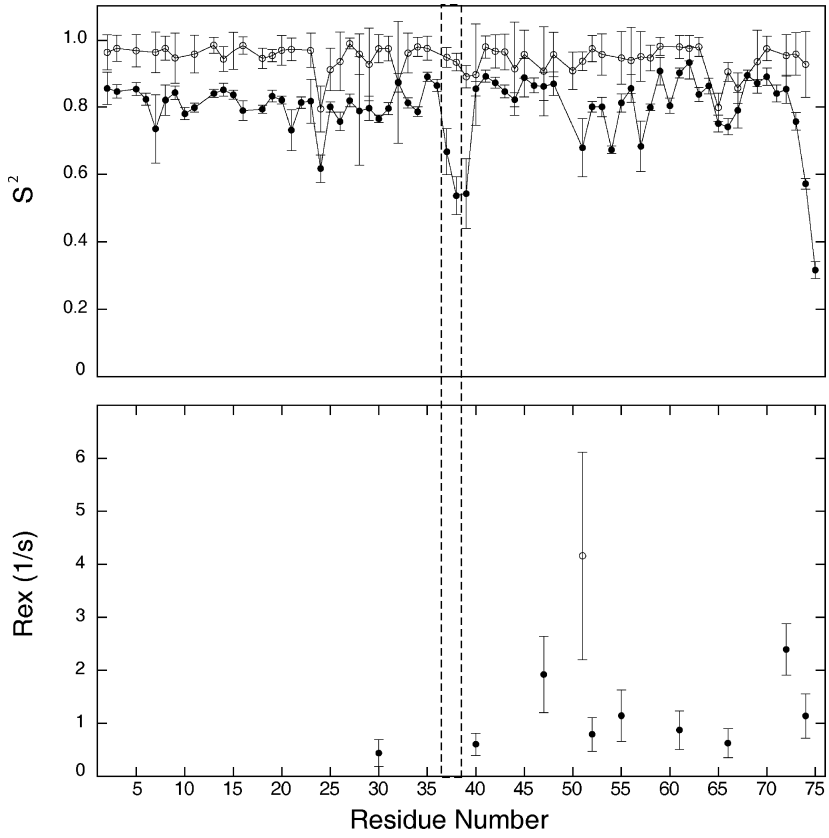

FIGURE 5: Backbone motion parameters of TCI. Order parameters (S^2) and contributions of exchange processes (R_{ex}) to the relaxation of backbone ^{15}N nuclei are represented vs the sequence of TCI, free (●) and in complex with hCPB (○). The vertical dotted lines indicate the limits between the two domains and the linker.

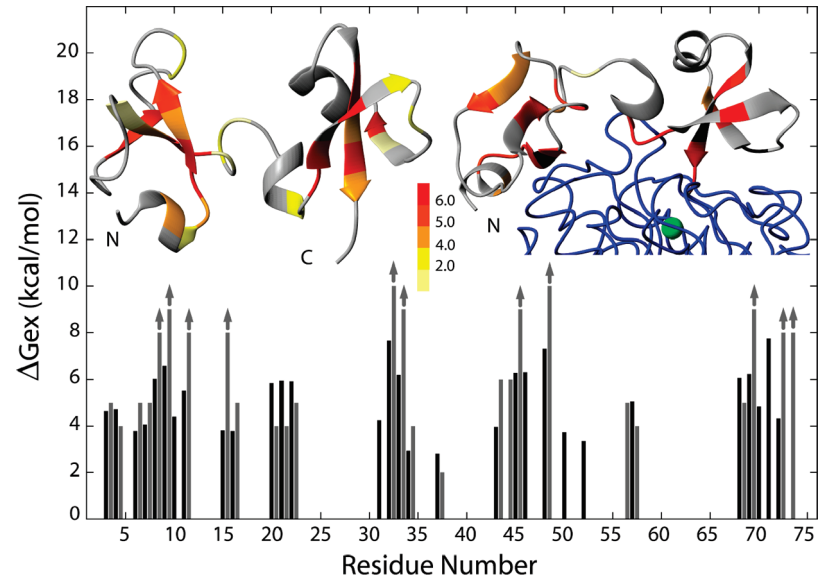

FIGURE 6: Free energy of exchange for TCI amide backbone protons. The plot shows the values of the free energy of exchange (ΔG_{ex}) vs residue number for TCI (black) and the TCI−hCPB complex (dark gray) at pH 5.5 and 298 K. The arrows label residues of the TCI−hCPB complex for which exchange was too slow to be reliably detected over a time period of 14 days and for which a lower limit of the exchange rate was estimated. The inset shows a ribbon diagram of TCI and the TCI−hCPB complex, with the catalytic zinc represented by a green sphere. Residues are colored according to the following color scheme: dark red, $\Delta G_{ex} \geq 6.0$ kcal/mol; pale red, $6.0 > \Delta G_{ex} \geq 5.0$; orange, $5.0 > \Delta G_{ex} \geq 4.0$; dark yellow, $4.0 > \Delta G_{ex} \geq 2.0$; and light yellow, $\Delta G_{ex} < 2.0$ kcal/mol.

The CSP values of the TCI backbone amides upon complex formation are generally higher for those residues that in the crystal structure of the complex are directly involved at the interface with hCPB than for the others. We also observed a tendency of residues with heavy atom intermolecular distances shorter than 6 Å in the crystal structure to experience large CSPs (Figure S5 of the Supporting Information). These findings indicate that the structure of the complex in solution is very similar to that in the crystal, since it is expected that the residues at the interface experience the strongest changes in their chemical environment. However, residues in the region of the interdomain linker display CSP values above the average, even though they do not form part of the interface (*16*). Thus,

they may experience a different chemical environment because of a conformational change or because of a loss of flexibility and stabilization of one of the various conformers populated in the free state. Other residues not directly involved in the binding interface, for example, Lys55 and Glu46, also exhibit large CSPs. This may be because they are affected by the ring currents of carboxypeptidase residues Tyr198 and Phe279 and by the change in orientation of the Trp73 indole ring in bound TCI with respect to its more variable orientation observed in the NMR ensemble (not shown). There were also large shifts in the signals of the $N_\epsilon H$ groups of arginine residues 52 and 21 (Figure 1). Arg52 is involved in a hydrogen bond with residue Thr164 in both hCPB and bCPA (*16*). On the other hand, the $N_\epsilon H$ group of Arg21 forms an intramolecular hydrogen bond (present in six of the 20 NMR structures) with the carbonyl group of Cys16 in the crystal structure of the TCI−hCPB complex. A stabilization of this hydrogen bond in the complex with respect to free TCI could explain the change in the signal of the $N_\epsilon H$ group of Arg21, although the low level of convergence of this local structural feature in the NMR ensemble of free TCI structures may also be due to the lack of NOEs involving the side chain of Arg21. These results show that the molecular recognition in solution is very similar to that observed in the crystal and that conformational changes occur, at least in the central region connecting the two domains. In agreement with this observation, the interaction interfaces between TCI bound to bCPA and bound to hCPB observed in the corresponding crystal structures were indistinguishable, but the positions of the two TCI domains relative to each other were slightly different (*16*).

Dynamics and Stability of TCI Free and Bound to hCPB. The backbone dynamics of TCI on the picosecond to millisecond time scales were examined by the spin relaxation properties of its amide ^{15}N nuclei. The residues at the C-terminus had smaller NOEs and longer T_1 and T_2 values, compared to those of most of the others (Figure 4), indicating flexibility on fast time scales (picoseconds to nanoseconds). These results indicate that the high rmsd value measured for the C-terminal residues was due to real flexibility; however, the imprecision in the structure at the level of the N-terminal residue may be caused by the absence of the corresponding amide proton and a preceding residue, reducing the number of measurable structural constraints. The S^2 values show that there is a general increase in order in TCI bound to hCPB compared with the free form (Figure 5), even in the cores of the two domains, the most rigid parts of free TCI. A similar overall increase in backbone order has been reported previously for a domain of the insulin-like growth factor binding protein upon binding to its receptor (*53*). However, relative to other regions of TCI, the three residues at the C-terminus are highly flexible in free TCI and become rigid in the complex. This is expected as the C-terminal end is inside the catalytic site of the carboxypeptidase in the crystal structure. The two residues of the linker and the first residue of the C-terminal domain (residues 37−39) also exhibited increased mobility in free TCI as compared with the residues at the core of the two domains. Also, this flexibility was significantly reduced upon complex formation. The region around residues 51−57 ($\beta 2_C$ and the previous and following loops), which is at the interaction interface, is also more flexible in solution and becomes rigid in the complex. By contrast, the region between residues 65 and 69 (the loop between $\alpha 2_C$ and $\beta 3_C$) is not directly involved in the interaction, and in the complex retains part of the flexibility demonstrated by the free form; this is also observed for Tyr24. Thus, although some regions become more rigid as a result of a direct interaction with the carboxypeptidase and others that do not interact remain relatively flexible, the linker becomes more rigid upon complex formation because both domains interact with their binding sites on the carboxypeptidase. This suggests that the inhibitor adjusts its structure to improve its interaction with the target peptidase.

Eight of the nine residues with slow motion-conformation exchange (R_{ex}) contributions to relaxation are located at the C-terminal domain in free TCI, but these contributions vanish when TCI is bound to hCPB (Figure 5). This suggests that certain local conformations taken up by the C-terminal domain chain on a microsecond to millisecond time scale became stabilized in the bound state. Therefore, although there is a general stabilization of the TCI structure in the complex, as shown by the S^2 values, this effect is more pronounced in the C-terminal domain. These results are consistent with there being less similarity among the C-terminal portions among the NMR ensemble than among N-terminal portions, similarly observed when comparing the free and bound structures (see Figure 3 and Tables 1 and 2).

According to the Linderstrøm−Lang model, the exchange reaction of a protected amide proton takes place when it is transiently exposed to the solvent as a result of a structural fluctuation (*54*). Because the amide protons of TCI exchange by an EX2 mechanism, the conformational fluctuation events in TCI do not necessarily lead to the exchange of the exposed amide protons; exchange itself is the limiting step of the reaction. Thus, backbone amide proton exchange with the solvent provides a window for observing main chain dynamics, and on time scales slower than that for ^{15}N relaxation data, because the exchange in folded polypeptide chains occurs over a much wider range, milliseconds to years. Exchange protection, relative to unfolded polypeptide chains, is interpreted in terms of participation in hydrogen bonds (secondary structure) or solvent inaccessibility (burial in the core). Exchange is thus facilitated by local unfolding or structural rearrangement events. In free TCI, most of the amide protons that are detected in D_2O are involved in hydrogen bonds (20 of 31), and most are located in regular secondary structure elements (Figure 2A). A clear exception is helix $\alpha 2_C$; the residues of this helix are lost in the first HSQC experiment even though four amide protons are consistently involved in hydrogen bonds in the NMR ensemble of structures. This observation suggests that the backbone has increased flexibility in this region on the millisecond to minute time scale.

Figure 6 shows the values of ΔG_{ex} that could be measured for TCI residues free and bound to hCPB. In both states, the residues with the highest values of ΔG_{ex} are located in the antiparallel β-sheets that form the cores of the two domains. With an EX2 mechanism, the exchange rates can be used to calculate the constant of the equilibrium between the open and closed forms of the protein, and in this case, the free energy of exchange is equivalent to the free energy of the opening reaction. TCI is the MCP inhibitor with the highest number of disulfide bonds, six versus the three and four disulfides displayed, respectively, by PCI and LCI.

These bonds strongly constrain the TCI structure and contribute to its extremely high stability against temperature and denaturing agents, resisting up to 90 °C (*14*) or up to 5.4 M guanidine hydrochloride under reducing conditions (*15*). However, this characteristic also hinders the measurement of free energy changes for the global unfolding of TCI, if global unfolding occurs in TCI under native, nonreducing conditions. An approximation of this value could be the ΔG_{ex} measured for the slowest exchanging amide protons (residues 32 and 71 in each of the two domains), 7.5 kcal/mol. If this value reflects the global unfolding event of each domain, there is no clear difference in their stabilities. However, the C-terminal domain was measured to be more stable than the N-terminal domain by chemical denaturation under reducing conditions; this suggests that either no global unfolding event occurs under native conditions or the stability under reducing conditions does not reflect the stability under native conditions. The comparison of ΔG_{ex} values between TCI and the TCI−hCPB complex shows that the structure of TCI is strongly stabilized upon complex formation, with a number of residues for which only a lower limit for ΔG_{ex} could be estimated (different for each residue due to their different intrinsic exchange rates; see Materials and Methods). The ΔG_{ex} comparison is consistent with the stabilization detected by the ^{15}N dynamics, but on a different time scale, as explained above. However, the stabilization is not homogeneous along the TCI chain. The amide protons of helix $\alpha 2_C$, located on the opposite side of the interaction interface, show no increased level of protection in the complex, and strand $\beta 2_N$, not directly involved in the interaction, appears to exchange slightly faster in the complex than if the protein is free. Thus, binding produces different changes in dynamics in distinct regions of TCI. Further studies of TCI dynamics in complex with other carboxypeptidases may shed light on the importance of these differences for the recognition of alternate enzymes.

Functional Insights and Implications. While the structure of free TCI is similar to that bound to hCPB, there are large differences in relation to internal dynamics, with the linker and the C-terminal domain becoming more rigid on binding hCPB. This is consistent with the proposed mechanism for the recognition of carboxypeptidases by TCI, which is thought to interact primarily with the enzyme through its C-terminal domain, whereas residues belonging to both domains further stabilize the complex by interacting with other parts of the carboxypeptidase. The flexibility of the linker allows the inhibitor to adjust the position of its two domains relative to each other, improving its interaction with the carboxypeptidase. Furthermore, the observed differences between the relative positions of the two domains in the crystal structures of the complexes with bCPA and hCPB suggest that this adaptability enables TCI to tune its global conformation for proper interaction with various types of carboxypeptidases. This mechanism of induced fit is reminiscent of a strategy recently introduced in drug design, called "tethering", in which synthetic inhibitors are optimized by combining a small fragment that binds to the enzyme active site with an adaptable exosite ligand (*55*).

TCI appears to be the best-evolved MCP inhibitor in terms of activity. Its two-domain fold, mimicking the duplication of two PCI or LCI molecules, provides it with the highest inhibition potential against A/B carboxypeptidases ($K_i = 1.3$ nM toward hCPB) (*14*). Elimination of the N-terminal half accounts for an important loss of inhibitory activity (~30 times) in comparison with the whole protein (*15*). Interestingly, other examples of double-headed inhibitors with improved affinity are found for thrombin, a key protease in blood coagulation (*56*). The plasticity of TCI at the level of the linker and the C-terminal domain makes it an ideal scaffold for developing stronger and/or more specific inhibitors directed toward modulating the activity of MCPs, especially that of TAFI. In this regard, the minor inhibition of fibrinolysis caused by small doses of TCI and its strong profibrinolytic effect, compared with other organic and proteinaceous carboxypeptidase inhibitors like 2-guanidinoethylmercaptosuccinic acid and PCI (*14*), is particularly relevant. These unique profibrinolytic properties of TCI may be therapeutically important for the prevention or treatment of thrombolytic disorders.

ACKNOWLEDGMENT

We gratefully acknowledge Ramón Campos-Olivas for helpful suggestions and discussions regarding relaxation measurements and analysis, as well as critical reading of the manuscript. We also thank José Luis Neira for advice on the measurement and interpretation of the exchange data and Guillermo Montoya for critical reading of the manuscript.

SUPPORTING INFORMATION AVAILABLE

A discussion on the exchange mechanisms and their distinction is included; figures showing a NOE-based contact map of free TCI in solution, the linearity of the exchange rates measured at two pH values, the distribution of TCI backbone dihedral angles in the ensemble of NMR structures and in its complex with hCPB and bCPA, the chemical shift perturbations of the TCI amide protons upon binding to hCPB, and the distribution of short distances in the crystal structure of its complex with hCPB, and two tables listing the measured exchange rates, the calculated intrinsic exchange rates, and the calculated free energies for exchange of the amide protons of TCI in its free and bound forms. This material is available free of charge via the Internet at http://pubs.acs.org.

REFERENCES

1. Arolas, J. L., Vendrell, J., Aviles, F. X., and Fricker, L. D. (2007) Metallocarboxypeptidases: Emerging drug targets in biomedicine. *Curr. Pharm. Des. 13*, 347–364.
2. Wei, S., Segura, S., Vendrell, J., Aviles, F. X., Lanoue, E., Day, R., Feng, Y., and Fricker, L. D. (2002) Identification and characterization of three members of the human metallocarboxypeptidase gene family. *J. Biol. Chem. 277*, 14954–14964.
3. Reznik, S. E., and Fricker, L. D. (2001) Carboxypeptidases from A to Z: Implications in embryonic development and Wnt binding. *Cell. Mol. Life Sci. 58*, 1790–1804.
4. Wei, S., Feng, Y., Kalinina, E., and Fricker, L. D. (2003) Neuropeptide-processing carboxypeptidases. *Life Sci. 73*, 655–662.
5. Kalinina, E., Biswas, R., Berezniuk, I., Hermoso, A., Aviles, F. X., and Fricker, L. D. (2007) A novel subfamily of mouse cytosolic carboxypeptidases. *FASEB J. 21*, 836–850.
6. Rodriguez de la Vega, M., Sevilla, R. G., Hermoso, A., Lorenzo, J., Tanco, S., Diez, A., Fricker, L. D., Bautista, J. M., and Aviles, F. X. (2007) Nna1-like proteins are active metallocarboxypeptidases of a new and diverse M14 subfamily. *FASEB J. 21*, 851–865.
7. Turk, B. (2006) Targeting proteases: Successes, failures and future prospects. *Nat. Rev. Drug Discovery 5*, 785–799.
8. Pallares, I., Bonet, R., Garcia-Castellanos, R., Ventura, S., Aviles, F. X., Vendrell, J., and Gomis-Ruth, F. X. (2005) Structure of

human carboxypeptidase A4 with its endogenous protein inhibitor, latexin. *Proc. Natl. Acad. Sci. U.S.A. 102*, 3978–3983.
9. Arolas, J. L., Bronsoms, S., Lorenzo, J., Aviles, F. X., Chang, J. Y., and Ventura, S. (2004) Role of kinetic intermediates in the folding of leech carboxypeptidase inhibitor. *J. Biol. Chem. 279*, 37261–37270.
10. Arolas, J. L., Lorenzo, J., Rovira, A., Vendrell, J., Aviles, F. X., and Ventura, S. (2004) Secondary binding site of the potato carboxypeptidase inhibitor. Contribution to its structure, folding, and biological properties. *Biochemistry 43*, 7973–7982.
11. Rees, D. C., and Lipscomb, W. N. (1982) Refined crystal structure of the potato inhibitor complex of carboxypeptidase A at 2.5 Å resolution. *J. Mol. Biol. 160*, 475–498.
12. Gonzalez, C., Neira, J. L., Ventura, S., Bronsoms, S., Rico, M., and Aviles, F. X. (2003) Structure and dynamics of the potato carboxypeptidase inhibitor by ^{1}H and ^{15}N NMR. *Proteins 50*, 410–422.
13. Reverter, D., Fernandez-Catalan, C., Baumgartner, R., Pfander, R., Huber, R., Bode, W., Vendrell, J., Holak, T. A., and Aviles, F. X. (2000) Structure of a novel leech carboxypeptidase inhibitor determined free in solution and in complex with human carboxypeptidase A2. *Nat. Struct. Biol. 7*, 322–328.
14. Arolas, J. L., Lorenzo, J., Rovira, A., Castella, J., Aviles, F. X., and Sommerhoff, C. P. (2005) A carboxypeptidase inhibitor from the tick *Rhipicephalus bursa*: Isolation, cDNA cloning, recombinant expression, and characterization. *J. Biol. Chem. 280*, 3441–3448.
15. Arolas, J. L., Bronsoms, S., Ventura, S., Aviles, F. X., and Calvete, J. J. (2006) Characterizing the tick carboxypeptidase inhibitor: Molecular basis for its two-domain nature. *J. Biol. Chem. 281*, 22906–22916.
16. Arolas, J. L., Popowicz, G. M., Lorenzo, J., Sommerhoff, C. P., Huber, R., Aviles, F. X., and Holak, T. A. (2005) The three-dimensional structures of tick carboxypeptidase inhibitor in complex with A/B carboxypeptidases reveal a novel double-headed binding mode. *J. Mol. Biol. 350*, 489–498.
17. Cai, M., Huang, Y., Sakaguchi, K., Clore, G. M., Gronenborn, A. M., and Craigie, R. (1998) An efficient and cost-effective isotope labeling protocol for proteins expressed in *Escherichia coli*. *J. Biomol. NMR 11*, 97–102.
18. Barbosa Pereira, P. J., Segura-Martin, S., Oliva, B., Ferrer-Orta, C., Aviles, F. X., Coll, M., Gomis-Ruth, F. X., and Vendrell, J. (2002) Human procarboxypeptidase B: Three-dimensional structure and implications for thrombin-activatable fibrinolysis inhibitor (TAFI). *J. Mol. Biol. 321*, 537–547.
19. Sattler, M., Schleucher, J., and Griesinger, C. (1999) Heteronuclear multidimensional NMR experiments for the structure determination of proteins in solution employing pulsed field gradients. *Prog. Nucl. Magn. Reson. Spectrosc. 34*, 93–158.
20. Delaglio, F., Grzesiek, S., Vuister, G. W., Zhu, G., Pfeifer, J., and Bax, A. (1995) NMRPipe: A multidimensional spectral processing system based on UNIX pipes. *J. Biomol. NMR 6*, 277–293.
21. Johnson, B. A., and Blevins, R. A. (1994) NMRView: A computer program for the visualization and analysis of NMR data. *J. Biomol. NMR 4*, 603–614.
22. Wishart, D. S., Bigam, C. G., Yao, J., Abildgaard, F., Dyson, H. J., Oldfield, E., Markley, J. L., and Sykes, B. D. (1995) ^{1}H, ^{13}C and ^{15}N chemical shift referencing in biomolecular NMR. *J. Biomol. NMR 6*, 135–140.
23. Palacios, A., Garcia, P., Padro, D., Lopez-Hernandez, E., Martin, I., and Blanco, F. J. (2006) Solution structure and NMR characterization of the binding to methylated histone tails of the plant homeodomain finger of the tumour suppressor ING4. *FEBS Lett. 580*, 6903–6908.
24. Herrmann, T., Guntert, P., and Wuthrich, K. (2002) Protein NMR structure determination with automated NOE assignment using the new software CANDID and the torsion angle dynamics algorithm DYANA. *J. Mol. Biol. 319*, 209–227.
25. Guntert, P., Mumenthaler, C., and Wuthrich, K. (1997) Torsion angle dynamics for NMR structure calculation with the new program DYANA. *J. Mol. Biol. 273*, 283–298.
26. Guntert, P. (2004) Automated NMR structure calculation with CYANA. *Methods Mol. Biol. 278*, 353–378.
27. Guntert, P., Braun, W., and Wuthrich, K. (1991) Efficient computation of three-dimensional protein structures in solution from nuclear magnetic resonance data using the program DIANA and the supporting programs CALIBA, HABAS and GLOMSA. *J. Mol. Biol. 217*, 517–530.
28. Pantoja-Uceda, D., Lopez-Mendez, B., Koshiba, S., Inoue, M., Kigawa, T., Terada, T., Shirouzu, M., Tanaka, A., Seki, M., Shinozaki, K., Yokoyama, S., and Guntert, P. (2005) Solution structure of the rhodanese homology domain At4g01050(175−295) from *Arabidopsis thaliana*. *Protein Sci. 14*, 224–230.
29. Case, D. A., Cheatham, T. E., III, Darden, T., Gohlke, H., Luo, R., Merz, K. M., Jr., Onufriev, A., Simmerling, C., Wang, B., and Woods, R. J. (2005) The Amber biomolecular simulation programs. *J. Comput. Chem. 26*, 1668–1688.
30. Laskowski, R. A., Rullmannn, J. A., MacArthur, M. W., Kaptein, R., and Thornton, J. M. (1996) AQUA and PROCHECK-NMR: Programs for checking the quality of protein structures solved by NMR. *J. Biomol. NMR 8*, 477–486.
31. Koradi, R., Billeter, M., and Wuthrich, K. (1996) MOLMOL: A program for display and analysis of macromolecular structures. *J. Mol. Graphics 14*, 51–55, 29−32.
32. Farrow, N. A., Muhandiram, R., Singer, A. U., Pascal, S. M., Kay, C. M., Gish, G., Shoelson, S. E., Pawson, T., Forman-Kay, J. D., and Kay, L. E. (1994) Backbone dynamics of a free and phosphopeptide-complexed Src homology 2 domain studied by ^{15}N NMR relaxation. *Biochemistry 33*, 5984–6003.
33. Renner, C., Schleicher, M., Moroder, L., and Holak, T. A. (2002) Practical aspects of the 2D ^{15}N-[^{1}H]-NOE experiment. *J. Biomol. NMR 23*, 23–33.
34. Johnson, B. A. (2004) Using NMRView to visualize and analyze the NMR spectra of macromolecules. *Methods Mol. Biol. 278*, 313–352.
35. Pawley, N. H., Wang, C., Koide, S., and Nicholson, L. K. (2001) An improved method for distinguishing between anisotropic tumbling and chemical exchange in analysis of ^{15}N relaxation parameters. *J. Biomol. NMR 20*, 149–165.
36. Tjandra, N., Feller, S. E., Pastor, R. W., and Bax, A. (1995) Rotational diffusion anisotropy of human ubiquitin from ^{15}N NMR relaxation. *J. Am. Chem. Soc. 117*, 12562–12566.
37. Bruschweiler, R., Liao, X., and Wright, P. E. (1995) Long-range motional restrictions in a multidomain zinc-finger protein from anisotropic tumbling. *Science 268*, 886–889.
38. Lipari, G., and Szabo, A. (1982) Model-free approach to the interpretation of nuclear magnetic resonance relaxation in macromolecules. 2. Analysis of experimental results. *J. Am. Chem. Soc. 104*, 4559–4570.
39. Cole, R., and Loria, J. P. (2003) FAST-Modelfree: A program for rapid automated analysis of solution NMR spin-relaxation data. *J. Biomol. NMR 26*, 203–213.
40. Palmer, A. G., Rance, M., and Wright, P. E. (1991) Intramolecular motions of a zinc finger DNA-binding domain from Xfin characterized by proton-detected natural abundance carbon-13 heteronuclear NMR spectroscopy. *J. Am. Chem. Soc. 113*, 4371–4380.
41. Mori, S., Abeygunawardana, C., Johnson, M. O., and van Zijl, P. C. (1995) Improved sensitivity of HSQC spectra of exchanging protons at short interscan delays using a new fast HSQC (FHSQC) detection scheme that avoids water saturation. *J. Magn. Reson., Ser. B 108*, 94–98.
42. Zhang, Y.-Z. (2007) Protein and peptide structure and interactions studied by hydrogen exchange and NMR. Ph.D. Thesis, University of Pennsylvania, Philadelphia.
43. Bartels, C., Billeter, M., Güntert, P., and Wüthrich, K. (1996) Automated sequence-specific NMR assignment of homologous proteins using the program GARANT. *J. Biomol. NMR 7*, 207–213.
44. Jung, Y. S., and Zweckstetter, M. (2004) Mars: Robust automatic backbone assignment of proteins. *J. Biomol. NMR 30*, 11–23.
45. Zimmerman, D. E., Kulikowski, C. A., Huang, Y., Feng, W., Tashiro, M., Shimotakahara, S., Chien, C., Powers, R., and Montelione, G. T. (1997) Automated analysis of protein NMR assignments using methods from artificial intelligence. *J. Mol. Biol. 269*, 592–610.
46. Wüthrich, K. (1986) *NMR of proteins and nucleic acids*, Wiley-Interscience, New York.
47. Schubert, M., Labudde, D., Oschkinat, H., and Schmieder, P. (2002) A software tool for the prediction of Xaa-Pro peptide bond conformations in proteins based on ^{13}C chemical shift statistics. *J. Biomol. NMR 24*, 149–154.
48. Vuister, G. W., and Bax, A. (1993) Quantitative J correlation: A new approach for measuring homonuclear three-bond J($H^{N}H^{\alpha}$) coupling constants in ^{15}N-enriched proteins. *J. Am. Chem. Soc. 115*, 7772–7777.
49. Cornilescu, G., Delaglio, F., and Bax, A. (1999) Protein backbone angle restraints from searching a database for chemical shift and sequence homology. *J. Biomol. NMR 13*, 289–302.

50. Neira, J. L., Sevilla, P., Menendez, M., Bruix, M., and Rico, M. (1999) Hydrogen exchange in ribonuclease A and ribonuclease S: Evidence for residual structure in the unfolded state under native conditions. *J. Mol. Biol. 285*, 627–643.
51. Skelton, N. J., Kordel, J., Akke, M., and Chazin, W. J. (1992) Nuclear magnetic resonance studies of the internal dynamics in Apo, $(Cd^{2+})_1$ and $(Ca^{2+})_2$ calbindin D9k. The rates of amide proton exchange with solvent. *J. Mol. Biol. 227*, 1100–1117.
52. Torres, A. M., and Kuchel, P. W. (2004) The β-defensin-fold family of polypeptides. *Toxicon 44*, 581–588.
53. Renner, C., and Holak, T. (2001) NMR ^{15}N relaxation of the insulin-like growth factor (IGF)-binding domain of IGF binding protein-5 (IGFBP-5) determined free in solution and in complex with IGF-II. *Eur. J. Biochem. 268*, 1058–1065.
54. Linderstrøm-Lang, K. U. (1955) Deuterium exchange between peptides and water. *Spec. Publ.—Chem. Soc. 2*, 1–20.
55. Erlanson, D. A., Wells, J. A., and Braisted, A. C. (2004) Tethering: Fragment-based drug discovery. *Annu. Rev. Biophys. Biomol. Struct. 33*, 199–223.
56. van de Locht, A., Lamba, D., Bauer, M., Huber, R., Friedrich, T., Kroger, B., Hoffken, W., and Bode, W. (1995) Two heads are better than one: Crystal structure of the insect derived double domain Kazal inhibitor rhodniin in complex with thrombin. *EMBO J. 14*, 5149–5157.
57. Holm, L., and Park, J. (2000) DaliLite workbench for protein structure comparison. *Bioinformatics 16*, 566–567.

BI800403M